# Magnitudes and Orientations of $^{31}$P Chemical Shielding Tensors in Pt(II)−Phosphine Complexes and Other Four-Fold Coordinated Phosphorus Sites

**Matthias Bechmann,[†,‡] Stephan Dusold,[†] Franz Geipel,[§] Angelika Sebald,*[,†,‡] and Dieter Sellmann[§,||]**

*Bayerisches Geoinstitut, Universität Bayreuth, D-95440 Bayreuth, Germany, and Institut für Anorganische Chemie II, Universität Erlangen, Egerlandstr. 1, D-91058 Erlangen, Germany*

*Received: October 11, 2004; In Final Form: March 26, 2005*

$^{31}$P MAS and double-quantum filtered $^{31}$P MAS NMR experiments at and near the $n = 0$ rotational resonance condition, as well as off-magic angle spinning $^{31}$P NMR experiments on two polycrystalline samples of Pt(II)−phosphine thiolate complexes are reported. Numerical simulations yield complete descriptions of the two $^{31}$P spin pairs. $^{195}$Pt MAS NMR spectra are straightforward to obtain but sensitively reflect only some parameters of the $^{195}$Pt($^{31}$P)$_2$ three-spin system. Based on the $^{31}$P NMR results obtained and in conjunction with a large body of literature data and irrespective of the chemical nature of the specimen, a unified picture of the dominating motif of $^{31}$P chemical shielding tensor orientations of phosphorus sites with 4-fold coordination is identified as a local (pseudo)plane rather than the directions of P element bond directions.

## Introduction

Small isolated spin systems play an important role in the context of many contemporary solid-state NMR approaches, ranging from applications aiming at structure elucidation to the evaluation of the performance of newly developed pulse sequences. Isolated homonuclear $^{31}$P spin pairs occur, for instance, in molecular fragments P−M−P in transition-metal−phosphine complexes. If M happens to be a magnetically active isotope, then the P−M−P fragment represents an isolated three-spin system. It is usually straightforward to obtain high-quality experimental $^{31}$P solid-state NMR spectra of these (and similar) spin systems in polycrystalline samples. The more challenging aspects are concerned with the extraction of the full set of unknown parameters describing these spin systems. Analysis of such experimental $^{31}$P NMR spectra requires numerically exact spectral line shape simulations in conjunction with iterative fitting procedures. The challenge for $^{31}$P spin systems mainly arises as a consequence of the 100 percent natural abundance of the isotope $^{31}$P, causing the need to determine simultaneously relatively large numbers of unknown parameters even for small spin systems.

Here we take the *cis*-PtP$_2$ fragment in two square-planar Pt(II)−phosphine complexes as representative examples. The spin $^1/_2$ isotope $^{195}$Pt has a natural abundance of 33.8%. Accordingly, the PtP$_2$ fragment consists of 33.8% isotopomers containing a ($^{31}$P)$_2$($^{195}$Pt) three-spin system and 66.2% ($^{31}$P)$_2$ spin-pair isotopomers. Typical orders of magnitude of the NMR interactions in the *cis*-PtP$_2$ fragment are as follows. Chemical shielding anisotropies are of the order $10^3$−$10^4$ Hz ($^{31}$P) or $10^5$ Hz ($^{195}$Pt) for common external magnetic field strengths, homonuclear $^{31}$P−$^{31}$P and heteronuclear $^{195}$Pt-$^{31}$P direct dipolar coupling constants both are of the order $10^2$ Hz, magnitudes of indirect heteronuclear dipolar coupling constants $^1J_{iso}$($^{195}$Pt, $^{31}$P) are of the order $10^3$ Hz, whereas indirect homonuclear dipolar coupling constants $^2J_{iso}$($^{31}$P,$^{31}$P) are of the order $10^0$−$10^1$ Hz and may have either positive or negative sign.[1,2] The anisotropy of indirect dipolar coupling $^{31}$P−$^{31}$P may be neglected, but the anisotropy of indirect dipolar coupling $^{195}$Pt−$^{31}$P may amount to the order of $10^3$ Hz and thus may exceed the magnitude of the corresponding direct dipolar coupling constants.

The two compounds containing *cis*-PtP$_2$ fragments chosen for this study represent one case for which the crystal structure is not known (compound **1**) whereas the crystal structure of compound **2** is known (Figure 1). $^{31}$P MAS NMR spectra with and without double-quantum filtration (DQF), as well as $^{31}$P NMR spectra obtained under off-magic-angle spinning (OMAS) conditions serve as the basis for the determination of all $^{31}$P NMR parameters in **1** and **2**. In addition, we consider briefly $^{195}$Pt MAS NMR spectra of **1** and **2** and will discuss in more general terms the orientation of $^{31}$P chemical shielding tensors in molecular moieties with phosphorus in 4-fold coordination.

## Experimental Section

**Samples.** *Compound 1*. Following a published synthesis procedure,[3] pure **1** was obtained in 92% yield after recrystallization from $CH_2Cl_2$/$Et_2O$. Solution-state $^{31}$P NMR ($CD_2Cl_2$) of **1**: $\omega_{iso}^{CS} = -52.2$ ppm, $^1J_{iso}$($^{195}$ Pt,$^{31}$P) = 2702 Hz; $^{13}$C CP/MAS NMR of **1** (aromatic region): $\omega_{iso}^{CS} = -150.5$ ppm; −130.9 ppm ($^2J_{iso}$($^{195}$ Pt,$^{13}$C) = 63 Hz); −121.3 ppm.

*Compound 2*. Reaction of *cis*-($^n$Bu$_3$P)$_2$PtCl$_2$ with an equimolar amount of 1,2-dimercapato-benzene in $CH_2Cl_2$ in the presence of a small amount of $NEt_3$ at ambient conditions for 12 h yielded crude **2** after evaporation of the solvent. Pure **2** was obtained in 63% yield after recrystallization from MeOH at $T = 243$ K. Solution-state $^{31}$P NMR ($CD_2Cl_2$) of **2**: $\omega_{iso}^{CS} = 5.0$ ppm, $^1J_{iso}$($^{195}$Pt,$^{31}$P) = 2745 Hz; $^{13}$C CP/MAS NMR of **2** (aromatic region): $\omega_{iso}^{CS} = -149.8$ ppm and −146.8 ppm; −129.4 ppm ($^2J_{iso}$($^{195}$Pt, $^{13}$C) = 63 Hz) and −128.5 ppm ($^2J_{iso}$($^{195}$Pt,$^{13}$C) = 68 Hz); −121.5 ppm and −120.8 ppm. Crystals of **2** suitable

* Corresponding author. E-mail: sebald@e3.physik.uni-dortmund.de.
† Universität Bayreuth.
‡ Current address: Universität Dortmund, Fachbereich Physik, D-44221 Dortmund, Germany.
§ Universität Erlangen.
|| Deceased.

10.1021/jp045353p CCC: $30.25 
Published on Web 06/01/2005

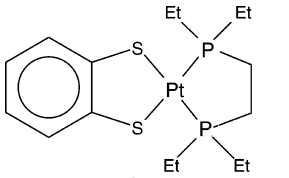


**1**

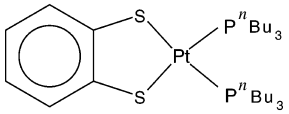


**2**

**Figure 1.** Schematic representation of molecules **1** and **2**.

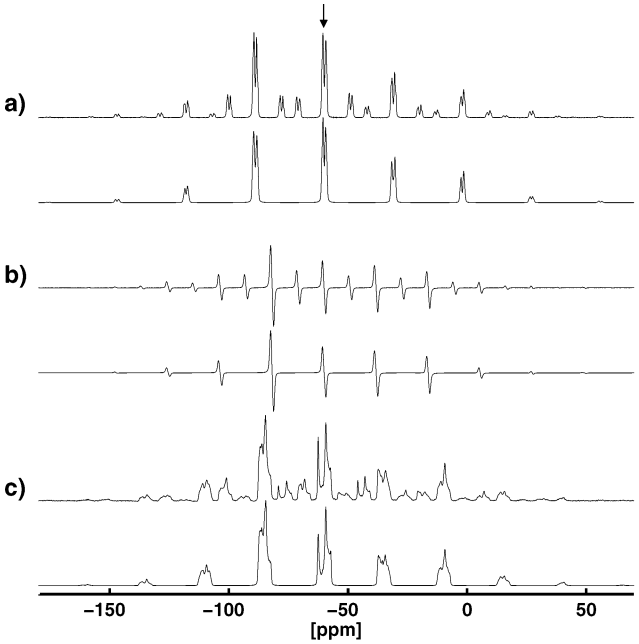


**Figure 2.** Experimental (upper traces) and best-fit simulated (lower traces) $^{31}$P NMR spectra of **1**. The arrow indicates the isotropic region of the $(^{31}P)_2$−isotopomer spectrum, simulated spectra only take the $(^{31}P)_2$ isotopomer into account. (a) $^{31}$P $n = 0$ $R^2$ MAS NMR, $\omega_0/2\pi = -121.5$ MHz, $\omega_r/2\pi = 3521$ Hz; (b) $R^2$-DQF $^{31}$P MAS NMR, $\omega_0/2\pi = -121.5$ MHz, $\omega_r/2\pi = 2650$ Hz, $\tau = 3.0$ ms, $\Delta = 3.5$ $\mu$s; (c) $^{31}$P OMAS NMR, $\omega_0/2\pi = -81.0$ MHz, $\omega_r/2\pi = 2028$ Hz, $\beta_{RL} = 56.023°$.

for structure determination by single-crystal X-ray diffraction were obtained by slow crystallization from a MeOH solution at room temperature. **2** crystallizes in space group *Pbca*,[4] the relevant internuclear distances are Pt−P1, 229.4 pm, and Pt−P2, 229.3 pm, and the P1−Pt−P2 bond angle is 98.0°. The molecular structure of **2** is depicted in Figure 4.

**$^{31}$P and $^{195}$Pt MAS NMR.** $^{31}$P MAS NMR spectra were recorded on Bruker MSL 100, MSL 200, MSL 300, and DSX 500 NMR spectrometers, equipped with standard 4 or 7 mm double-resonance double-bearing CP MAS probes. The corresponding $^{31}$P Larmor frequencies $\omega_0/2\pi$ are −40.5, −81.0, −121.5, and −202.5 MHz. Hartmann−Hahn cross polarization (CP) was used ($^1$H $\pi/2$-pulse durations 2.5−3.5 $\mu$s, recycle delays 3−5 s, and CP contact times 0.5−2.0 ms). Line shapes of experimental $^{31}$P MAS NMR spectra were checked to be identical when using either cross polarization or $^{31}$P single-pulse excitation. $^{31}$P chemical shielding is quoted with respect to $\omega_{iso}^{CS} = 0$ ppm for the $^{31}$P resonance of 85% H $_3PO_4$. $^{195}$Pt CP MAS NMR spectra were recorded on the MSL 100 (7 mm rotor, $\omega_0/2\pi = -21.4$ MHz) and MSL 200 (4 mm rotor, $\omega_0/2\pi = -42.8$ MHz) spectrometers, employing $^1$H $\pi/2$-pulse durations

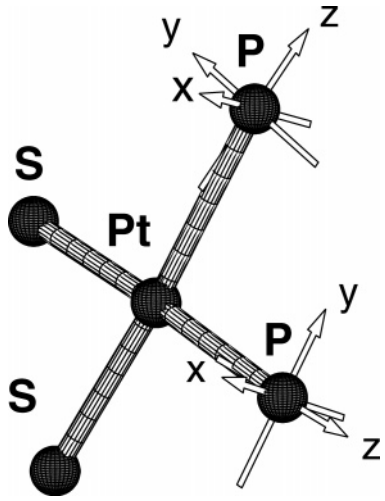


**Figure 3.** Illustration of the orientation of the $^{31}$P chemical shielding tensors in the $S_2PtP_2$ fragment of molecule **1**.

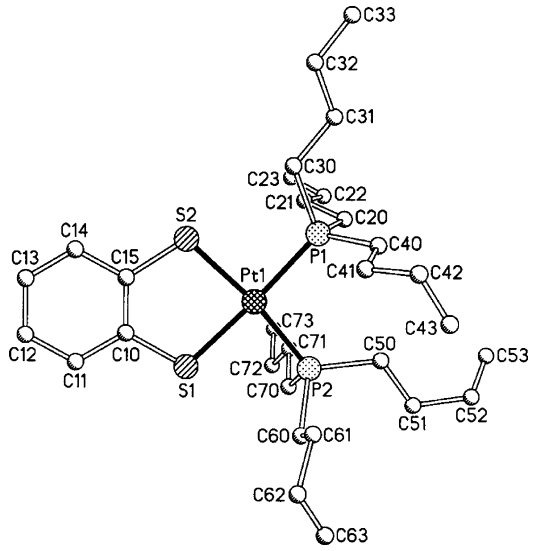


**Figure 4.** Molecular structure of solid **2** according to single-crystal X-ray diffraction.[4]

of 3.5−4.5 $\mu$s and CP contact times of 5 ms. $^{195}$Pt chemical shielding is given relative to $\Xi(^{195}Pt) = 21.4$ MHz.[5]

MAS frequencies were generally in the range $\omega_r/2\pi = 1-10$ kHz and were actively controlled to within ± 2 Hz. $^1$H c.w. decoupling with amplitudes in the range 55 kHz to 85 kHz was employed during signal acquisition. Special care was taken to adjust the magic angle $\beta_{RL} = \tan^{-1}\sqrt{2}$ for all MAS NMR experiments as accurately as possible by optimizing the line shape of the $^{31}$P resonance of $(Et_2\ P{=}S)_2$ under MAS conditions.[6] The shape of the $^{31}$P resonance of $P(C_6H_{11})_3$ served for calibration of the spinning angle in OMAS NMR experiments. For double-quantum filtration experiments the COSY-like sequence $CP_{(x)} - \tau - (\pi/2)_{(y)} - \Delta - (\pi/2)_{(\phi)} -$ acqusition was used[7] where $\phi$ indicates phase cycling suitable for DQF.[8] The duration of $\Delta$ was fixed as $\Delta = 3.5$ $\mu$s, the duration of $\tau$ was varied.

**Definitions, Notation, and Numerical Methods.** Shielding notation[9] is used throughout. For the interactions $\lambda$ = CS (chemical shielding), $\lambda$ = D (direct dipolar coupling), and $\lambda$ = J (indirect dipolar (*J*) coupling) the isotropic part $\omega_{iso}^{\lambda}$, the anisotropy $\omega_{aniso}^{\lambda}$, and the asymmetry parameter $\eta^{\lambda}$ relate to the principal elements of the interaction tensor $\omega^{\lambda}$ as follows:[10] $\omega_{iso}^{\lambda} = (\omega_{xx}^{\lambda} + \omega_{yy}^{\lambda} + \omega_{zz}^{\lambda})/3$, $\omega_{aniso}^{\lambda} = \omega_{zz}^{\lambda} - \omega_{iso}^{\lambda}$, and $\eta^{\lambda} = (\omega_{yy}^{\lambda}$

$-\omega_{xx}^{\lambda})/\omega_{\text{aniso}}^{\lambda}$ with $|\omega_{zz}^{\lambda}-\omega_{iso}^{\lambda}| \geq |\omega_{xx}^{\lambda}-\omega_{iso}^{\lambda}| \geq |\omega_{yy}^{\lambda}-\omega_{iso}^{\lambda}|$. For indirect dipolar coupling $\omega_{\text{iso}}^{J} = \pi J_{\text{iso}}$, and for direct dipolar coupling $\eta^{\text{D}} = \omega_{\text{iso}}^{\text{D}} = 0$ and $\omega_{\text{aniso}}^{\text{D}_{ij}} = b_{ij} = -\mu_0\gamma_i\gamma_j\hbar/(4\pi r_{ij}^3)$, where $\gamma_i$ and $\gamma_j$ denote gyromagnetic ratios and $r_{ij}$ is the internuclear distance between spins $S_i$ and $S_j$. $i, j = 1, 2$ refers to the homonuclear $(^{31}\text{P})_2$ part of the $(^{31}\text{P})_2(^{195}\text{Pt})$ three-spin system. The Euler angles $\Omega_{IJ} = \{\alpha_{IJ}, \beta_{IJ}, \gamma_{IJ}\}$ relate axis system $I$ to axis system $J$; $I,J$ denote P (principal axis system, PAS), C (crystal axis system, CAS), R (rotor axis system, RAS), or L (laboratory axis system).[11] In the context of MAS NMR experiments on the $(^{31}\text{P})_2(^{195}\text{Pt})$ spin system, it is convenient to define the PAS of $\omega^{\text{D}_{12}}$ as the CAS, $\Omega_{\text{PC}}^{\text{D}_{12}} = \{0, 0, 0\}$. Our procedures for numerically exact spectral line shape simulations and iterative fitting are fully described and discussed in detail elsewhere, in particular addressing the $n = 0$ rotational resonance ($R^2$) condition for isolated homonuclear spin pairs,[12,13] various $n = 0, 1, 2$ $R^2$ conditions in an isolated homonuclear four-spin system,[13] and different heteronuclear dipolar de- and recoupling MAS conditions for isolated heteronuclear two-[14] and three-spin systems.[15,16] For meaningful simulations of OMAS NMR spectra, larger sets of powder angles are needed (e.g., 700 sets of angles selected by REPULSION [17]) than in simulations of MAS NMR spectra (e.g., 232 sets).

## Results and Discussion

The following section is organized into three parts. First, we will discuss the experimental determination of the parameters of the $^{31}$P spin pairs in **1** and **2**. The second part will briefly describe $^{195}$Pt MAS NMR spectra of **1** and **2**. In the third part we will discuss general trends in the orientations of $^{31}$P chemical shielding tensors for phosphorus atoms in 4-fold coordination.

**$^{31}$P NMR of Solid 1 and 2.** Experimental options to generate $^{31}$P NMR spectra of polycrystalline powder samples containing the $PtP_2$ fragment include experiments on nonspinning samples, on samples spinning under off-magic-angle (OMAS) conditions, and on samples under MAS conditions with or without so-called dipolar recoupling[16] and/or double-quantum filtration techniques applied. With the exception of $^{31}$P NMR spectra of nonspinning samples of **1** and **2** here all these experimental techniques are used. Static powder patterns of samples such as **1** or **2**, containing not only isolated $^{31}$P spin pairs but also isotopomers $^{195}\text{Pt}(^{31}\text{P})_2$, are not a suitable starting point for the full characterization of the $^{31}$P spin pair as $^{31}$P spectral contributions from both isotopomers overlap heavily. This is not a problem for the simulation of spectra, but it would be a major problem for the extraction of multiple parameters from experimental spectra. Therefore, our data analysis is based on experimental data for which sample spinning provides a separation of the $^{31}$P spectral contributions from the two isotopomers.

**(i) $^{31}$P NMR of 1.** Inspection of a $^{13}$C MAS NMR spectrum of **1** is a good starting point for the analysis of $^{31}$P MAS NMR spectra of **1**. Only three sharp $^{13}$C resonances are observed for the aromatic thiolate ligand, indicating molecular symmetry (see the Experimental Section). Either a $C_2$ axis or a mirror plane bisecting the P−Pt−P angle are possible, both rendering the two phosphorus sites in a molecule of **1** crystallographically equivalent. The corresponding two $^{31}$P chemical shielding tensors thus represent a so-called $n = 0$ rotational resonance ($R^2$) condition[12,18] with identical isotropic chemical shielding values but nonidentical chemical shielding tensor orientations. The $n = 0$ rotational resonance $R^2$ condition gives rise to complicated spectral line shapes in which the magnitudes and orientations of all interaction tensors of the spin pair are usually sensitively encoded[12−14] at arbitrary spinning frequencies. A priori, in the absence of knowledge of the crystal structure of **1**, we do not know which of the two symmetry operations is present, and experimental $^{31}$P MAS NMR spectra of **1**, obtained at different MAS and Larmor frequencies, have to be fitted for either of the two possibilities. Note that the presence of a $C_2$ symmetry element is a special case for a spin pair as it defines the absolute orientation of the two $^{31}$P chemical shielding tensors[13] whereas a symmetry plane only defines their relative orientations, leaving free rotation of the tensors around the unique axis of the $^{31}$P−$^{31}$P dipolar coupling tensor possible.

**TABLE 1**

| | **1** ($C_2$)[a] | **1** ($\sigma$)[a] | **2** |
|---|---|---|---|
| $\omega_{iso}^{CS_1}$ [ppm] | −60.0 | −60.0 | +2.1 |
| $\omega_{iso}^{CS_2}$ [ppm] | −60.0 | −60.0 | +2.5 |
| $\omega_{aniso}^{CS_1}$ [ppm] | 78.0 ± 1 | 77.8 ± 1 | −57 ± 3 |
| $\omega_{aniso}^{CS_2}$ [ppm] | 78.0 ± 1 | 77.8 ± 1 | −68 ± 3 |
| $\eta^{CS_1}$ | 0.52 ± 0.02 | 0.50 ± 0.02 | 0.35 ± 0.1 |
| $\eta^{CS_2}$ | 0.52 ± 0.02 | 0.50 ± 0.02 | 0.35 ± 0.1 |
| $\alpha_{PC}^{CS_1}$ [°][b] | 90 ± 9 | 92 ± 9 | 95 ± 21 |
| $\beta_{PC}^{CS_1}$ [°][b] | 51 ± 3 | 45 ± 3 | 40 ± 11 |
| $\gamma_{PC}^{CS_1}$ [°][b] | 0 ± 3 | 0 | 43 ± 30 |
| $\alpha_{PC}^{CS_2}$ [°][b] | 90 ± 9 | −92 ± 9 | 49 ± 21 |
| $\beta_{PC}^{CS_2}$ [°][b] | 231 ± 3 | 88 ± 9 | 130 ± 10 |
| $\gamma_{PC}^{CS_2}$ [°][b] | 180 ± 3 | 0 | 0 |
| $^2J_{\text{iso}}(^{31}\text{P},^{31}\text{P})$ [Hz] | −9.3 ± 5 | −13.0 ± 5 | −23.0 ± 6 |
| $b_{12}/2\pi$ [Hz] | −708 ± 31 | −683 ± 31 | −475[c] |

[a] The Euler angles $\Omega_{\text{PC}}^{CS_{1,2}}$ are related by symmetry. If related by $C_2$ symmetry: $\alpha_{\text{PC}}^{CS_2} = \alpha_{\text{PC}}^{CS_1}$; $\beta_{\text{PC}}^{CS_2} = \beta_{\text{PC}}^{CS_1} + \pi$; $\gamma_{\text{PC}}^{CS_2} = -\gamma_{\text{PC}}^{CS_1} + \pi$. If related by a mirror plane $\sigma$: $\alpha_{\text{PC}}^{CS_2} = -\alpha_{\text{PC}}^{CS_1}$; $\beta_{\text{PC}}^{CS_2} = \pi - \beta_{\text{PC}}^{CS_1}$; $\gamma_{\text{PC}}^{CS_2} = \gamma_{\text{PC}}^{CS_1}$. [b] The Euler angles $\Omega_{\text{PC}}^{CS}$ are given relative to $\Omega_{\text{PC}}^{D_{12}} = \{0, 0, 0\}$ with the $x$ axis of the dipolar coupling tensor taken as parallel to the $C_2$ symmetry axis. [c] Calculated from the crystal structure.[4]

Figure 2a depicts a $^{31}$P MAS NMR spectrum of **1**, together with the corresponding final best-fit simulated spectrum. Iterative fitting of various different straightforward $^{31}$P MAS NMR spectra of **1** converges to identical solutions when assuming either of the two symmetry elements to be present. In principle the two different symmetries are distinguishable but they turn out indistinguishable for the $^{31}$P spin pair in **1** because of the values of the Euler angles being $\alpha_{\text{PC}}^{CS_1} = 90° \pm 9°$ and $\gamma_{\text{PC}}^{CS_1} = 0° \pm 3°$ (see Table 1). Iterative fitting of several $^{31}$P MAS NMR spectra of **1** defines, for instance, the set of angles $\Omega_{\text{PC}}^{CS_1} = \{87 \pm 11, 51 \pm 6, 0 \pm 6\}$. This result can be further improved by additional analyses of the $^{31}$P spectral line shapes obtained by applying a COSY-like pulse sequence with double-quantum filtration (DQF) under MAS conditions and by analyzing experimental spectra obtained under OMAS conditions. Experimental $^{31}$P $R^2$-DQF and OMAS NMR spectra of **1** are depicted in Figure 2, panels b and c, together with the corresponding best-fit simulations. $R^2$-DQF MAS NMR line shapes at and near the $n = 0$ $R^2$ condition are known to exhibit higher sensitivities toward anisotropic interaction parameters than conventional $R^2$ line shapes.[12] Spinning the sample at an angle $\beta_{\text{RL}} \neq \tan^{-1}\sqrt{2}$ (OMAS) leads to spinning sideband patterns where each sideband represents a scaled powder pattern, slightly different from the spinning sideband pattern obtained when spinning exactly at the magic angle.[19−23] With OMAS conditions only slightly deviating from the magic angle we find that often minima regions in error maps are more sharply defined than based on $R^2$ or $R^2$-DQF MAS NMR line shapes. The uncertainties of the data given in Table 1 are the combined constraints from fitting experimental $^{31}$P $R^2$ and $R^2$-DQF MAS as well OMAS spectra of **1**. Our $^{31}$P NMR data yield a P−P distance in **1** of 305 ± 2 pm, in excellent agreement with the

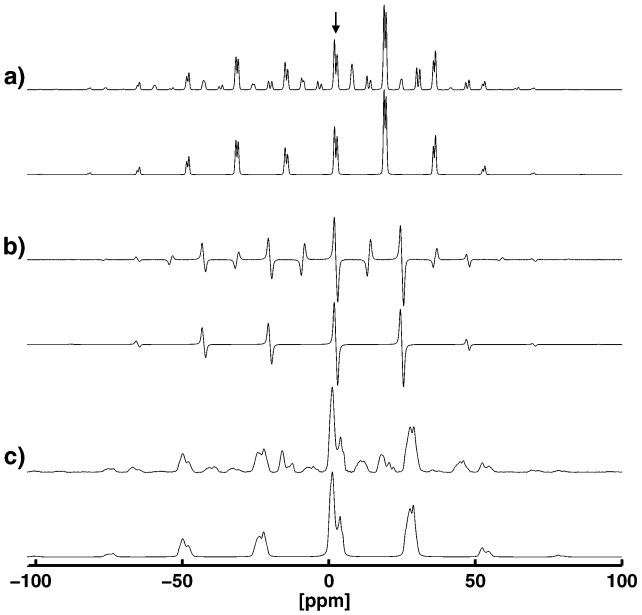


**Figure 5.** Experimental (upper traces) and best-fit simulated (lower traces) $^{31}$P NMR spectra of **2**. The arrow indicates the isotropic region of the $(^{31}P)_2$-isotopomer spectrum, simulated spectra only take the $(^{31}P)_2$ isotopomer into account. (a) $^{31}$P $n = 0$ $R^2$ MAS NMR, $\omega_0/2\pi = -121.5$ MHz, $\omega_r/2\pi = 2046$ Hz; (b) $R^2$-DQF $^{31}$P MAS NMR, $\omega_0/2\pi = -121.5$ MHz, $\omega_r/2\pi = 2740$ Hz, $\tau = 3.3$ ms, $\Delta = 3.5$ $\mu$s; (c) $^{31}$P OMAS NMR, $\omega_0/2\pi = -81.0$ MHz, $\omega_r/2\pi = 2075$ Hz, $\beta_{RL} = 56.196°$.

results of X-ray diffraction studies of numerous closely related compounds containing a *cis*-$S_2PtP_2$ moiety.[24]

Figure 3 illustrates the orientation of the two $^{31}$P chemical shielding tensors in the molecule **1**. For the $^{31}$P chemical shielding tensors in **1**, the *zz* component represents the *most* shielded direction and is oriented along the direction of the respective Pt−P bonds. For the moment, we leave the issue of the $^{31}$P chemical shielding tensor orientation at this stage but will return to this topic later (see below).

**(ii) $^{31}$P NMR of 2.** The starting point for the analysis of $^{31}$P MAS NMR spectra of **2** is the crystal structure. The molecular structure of solid **2** is shown in Figure 4. The two phosphorus sites in the molecule are not crystallographically equivalent and will thus give rise to two slightly different $^{31}$P resonances. In accordance with the crystal structure data, $^{13}$C MAS NMR spectra of **2** display six $^{13}$C resonances for the aromatic ring of the thiolate ligand (see the Experimental Section). From the known internuclear $^{31}$P−$^{31}$P distance in **2**, the corresponding dipolar coupling constant is calculated and does not have to be determined from iterative fitting of $^{31}$P MAS NMR spectra of **2**. Other than for **1**, however, in **2** there is no symmetry relationship between the two $^{31}$P chemical shielding tensors, and accordingly, simulations have to allow for a (small) difference in isotropic chemical shielding of the two resonances as well as for unrelated Euler angles describing the orientations of the two $^{31}$P chemical shielding tensors. Despite the known crystal structure, simulations of the $^{31}$P MAS NMR spectra of **2** involve more unknown parameters than was the case for **1**.

We follow the same procedure as before. After recording several different $^{31}$P $R^2$ and $R^2$-DQF MAS as well OMAS NMR spectra of **2** and combining all results, we obtain the data given in Table 1. These best-fit parameters yield the simulated spectra shown in Figure 5, together with the corresponding experimental $^{31}$P NMR spectra of **2**. Determination of the $^{31}$P chemical shielding values of **2**, representing a near $n = 0$ $^{31}$P $R^2$ spin system, particularly gains from $R^2$-DQF MAS NMR experiments

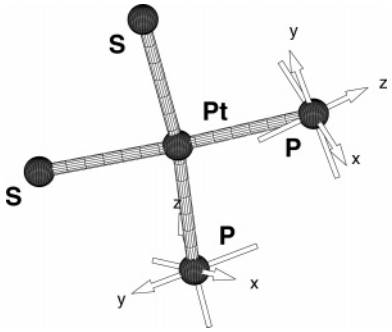


**Figure 6.** Illustration of the orientation of the $^{31}$P chemical shielding tensors in the $S_2PtP_2$ fragment of molecule **2**.

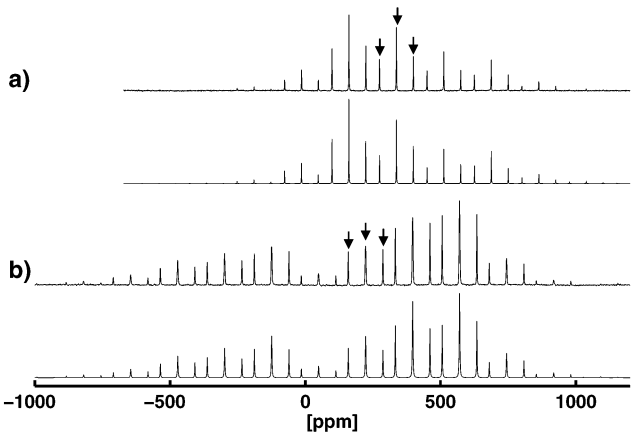


**Figure 7.** Experimental (upper traces) and simulated (lower traces) $^{195}$Pt MAS NMR spectra of **1** (a) and **2** (b); arrows indicate center band resonances, $\omega_0/2\pi = -42.8$ MHz. (a) $\omega_r/2\pi = 7449$ Hz; (b) $\omega_r/2\pi = 7439$ Hz.

where all orientational parameters are more sensitively encoded than in the conventional $R^2$ MAS or OMAS NMR spectra.[12] Note that for **1** and **2** the values as well as the signs of the isotropic *J*-coupling constants $^2J_{iso}(^{31}P,^{31}P)$ are well defined from the line shape analyses even if these *J* couplings are not resolved in the spectra and none of the splittings visible in some of the spectra directly depict these *J* couplings.

Again, just as before for **1** (see Figure 3), we illustrate the orientations of the two $^{31}$P chemical shielding tensors in **2** in Figure 6. Also for **2** the direction of the *zz* components of the two chemical shielding tensors nearly coincide with the directions of the corresponding Pt−P bond directions. However, in contrast to **1**, for **2** the *zz* components of the two chemical shielding tensors represent the *least* shielded components. We will return to this seeming puzzle below.

**$^{195}$Pt MAS NMR of 1 and 2.** $^{195}$Pt MAS NMR spectra of **1** and **2** are depicted in Figure 7. Given that we observe the X-part spectrum of the $^{195}Pt(^{31}P)_2$ three-spin systems in **1** and **2** and that we know all parameters of the $^{31}$P parts of these spin systems, one might expect to be able to fully characterize also the $^{195}$Pt part of the spin systems, provided some heteronuclear dipolar recoupling pulse sequence[16] is applied, or a sufficiently slow MAS rate is used so that the heteronuclear $^{195}$Pt−$^{31}$P direct dipolar coupling interactions are not completely averaged out.

Obviously (Figure 7), experimental $^{195}$Pt MAS NMR spectra of **1** and **2** are well reproduced by numerical simulations. Closer inspection of various experimental data, however, reveals that even at a low Larmor frequency $\omega_0/2\pi = -21.4$ MHz and at very slow spinning rates $\omega_r/2\pi \leq 800$ Hz, the only sensitively encoded fit parameters are the anisotropy of the $^{195}$Pt chemical shielding and the isotropic *J*-coupling constants $^1J_{iso}(^{195}Pt, ^{31}P)$.

In addition, it turns out that the spinning angle is a highly sensitive fit parameter: deviations from the magic angle as small as ±0.05° lead to significant changes in the spinning sideband patterns of these $^{195}$Pt MAS NMR spectra. This finding for MAS NMR spectra of spin-1/2 isotopes with very large chemical shielding anisotropies is familiar from MAS NMR experiments on quadrupolar nuclei where large quadrupolar interactions also lead to spectra being highly sensitive to the accurate setting of the magic angle.[25] Even if the large $^{195}$Pt chemical shielding anisotropy would not be the overwhelmingly large interaction parameter in the $^{195}$Pt($^{31}$P)$_2$ three-spin systems in **1** and **2**, we may be faced with another difficulty in determining the geometry of the $PtP_2$ moiety from $^{31}$P and $^{195}$Pt MAS NMR experiments. The values of the *J*-coupling constants $^1J_{iso}(^{195}Pt,^{31}P)$ in **1** and **2** are ca. 2700 Hz. Therefore, an anisotropy of this *J*-coupling interaction of a similar magnitude is likely to be present. $\omega^J_{aniso}$ may add to, or subtract from, the respective dipolar coupling constants, with the *J*-coupling tensor having an unknown orientation. This may then lead to an apparent dipolar coupling constant $b_{eff}$ which would not directly reflect the internuclear $^{195}$Pt−$^{31}$P distances, making it impossible to deduce these internuclear distances. In fact, it has been found earlier for the $CdP_2$ fragment in a Cd(II)−phophine complex that the heteronuclear $^{113}$Cd−$^{31}$P dipolar coupling and the anisotropy of the *J* coupling $^1J(^{113}Cd,^{31}P)$ essentially cancel each other.[15]

**$^{31}$P Chemical Shielding Tensor Orientations.** There is a fair number of $^{31}$P solid-state NMR studies in the literature in which $^{31}$P chemical shielding tensor orientations have been determined experimentally. $^{31}$P NMR experiments on oriented single crystals[14,26−43] as well as $^{31}$P NMR studies on polycrystalline powders[1,13−15,44−47] have been reported. Most often, the $^{31}$P chemical shielding tensor orientations are being discussed by describing the orientation of certain bond directions relative to the directions of the *xx*, *yy*, and *zz* components of the $^{31}$P chemical shielding tensors. Implicitly, we have so far followed this common practice (see Figures 3 and 6) by mentioning that in both **1** and **2** the $^{31}$P chemical shielding tensors are oriented such that the directions of their *zz* components nearly coincide with the respective Pt−P bond directions. This line of argument, however, leads to some confusion. Why should in one of these two very closely related compounds the *most* shielded direction coincide with Pt−P bond direction, and why should this be the *least* shielded direction in the second compound? Obviously, it is not the Pt−P bond direction that reveals the common pattern of these $^{31}$P chemical shielding tensor orientations.

Here it helps to consult results in the literature which cover a wide range in terms of chemistry, ranging from phosphorus in organophosphates and in inorganic phosphates all the way to phophorus in transition-metal phosphine complexes. All these diverse compounds have in common that the phosphorus atom is 4-fold coordinated in a more or less distorted tetrahedral $PE_4$ environment (E = C, O, S, Pt, Hg, Cd, ...). The corresponding $^{31}$P chemical shielding tensors also have something in common, irrespective of the chemical nature of the compounds. One can always find a local (pseudo)plane of symmetry, defined by the P atom and two of its neighbored atoms, and always the direction of one of the $^{31}$P chemical shielding tensor components is perpendicular to this plane. Sometimes the final result is such that one of the remaining two components of the $^{31}$P chemical shielding tensor will actually coincide with a molecular P−E bond direction (for example, in **1** and **2**), but the local plane is the dominating element in defining the $^{31}$P chemical shielding tensor orientation. Recasting our results on **1** and **2** in the light of a local plane as the determining element, immediately reveals the common property of the $^{31}$P chemical shielding tensors in these two compounds. Drawing a plane defined by the local coordination $PtPC_3$, containing the central P atom in its distorted tetrahedron environment, the platinum atom and the directly bonded carbon atom of one of the three organic substituents of the phosphine ligand, identifies that in both cases the direction of the intermediate *yy*-component of the $^{31}$P chemical shielding tensor is oriented perpendicular to this idealized local plane. This is illustrated in Figure 8.

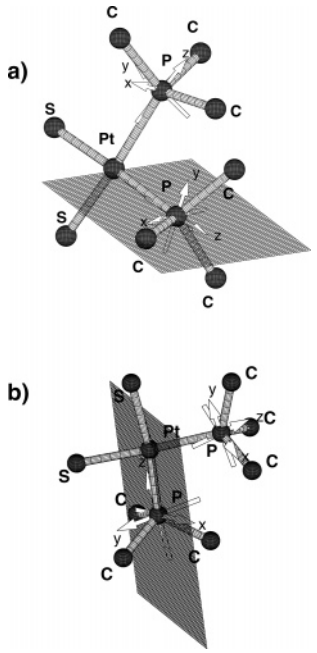


**Figure 8.** Orientations of the $^{31}$P chemical shielding tensors in **1** (a) and **2** (b) with the local planes defined by C−P−Pt shown; the directions of the intermediate *yy* components of the shielding tensors are perpendicular to these planes.

The determining role of a local plane in defining $^{31}$P chemical shielding tensor orientations becomes particularly clear from the example of an organic phosphate salt. The $^{31}$P chemical shielding tensor in tris-ammonium phosphoenolpyruvate[14] has a very small asymmetry parameter $\eta^{CS}$ and the P atom is in a nearly tetrahedral local $O_3PO-C$ coordination. Chemical intuition might thus suggest that the direction of the nearly unique *zz*-component of this $^{31}$P chemical shielding tensor should approximately coincide with the chemically distinct P−C bond direction in this $O_3PO-C$ moiety. This is not the case as is revealed by $^{31}$P single-crystal NMR, again it is a local plane spanned by two of the oxygen atoms and the phosphorus atom that marks the orientation of the $^{31}$P chemical shielding tensor, the directions of neither of the shielding tensor components coincide with a bond direction in this molecule.

## Summary and Conclusions

Combining $^{31}$P $R^2$ and $R^2$-DQF MAS NMR and OMAS NMR experiments provides a good database for the full characterization of $^{31}$P spin pairs in polycrystalline powder samples by line shape analysis. Even if not necessary for reasons of background-signal suppression, $R^2$-DQF MAS experiments and in particular OMAS NMR spectra are a useful complement to conventional $R^2$ MAS NMR experiments in that these additional experiments display different, and often higher, sensitivities to the various anisotropic interaction parameters of the spin pair. Owing to the very large $^{195}$Pt chemical shielding anisotropies and the

**TABLE 2: $^{195}$Pt NMR Data of 1 and 2**

| | 1 | 2 |
|---|---|---|
| $\omega_{iso}^{CS}$ [ppm] | 338 | 225 |
| $\omega_{aniso}^{CS}$ [ppm] | 550 | −907 |
| $\eta^{CS}$ | 0.4 | 0.1 |
| $^1J_{iso}(^{195}Pt,^{31}P)$ [Hz] | 2666 | 2708; 2772 |

unknown anisotropies of the *J* couplings $^1J(^{195}Pt,^{31}P)$ it turns out impossible to derive the orientation of the $^{195}$Pt chemical shielding tensor in molecular fragments $P_2Pt$ from $^{195}$Pt MAS NMR experiments, although good quality $^{195}$Pt MAS NMR spectra are easily obtained. From the $^{31}$P NMR results on **1** and **2** and from numerous literature data a unified picture concerning the dominating motif of the orientation of $^{31}$P chemical shielding tensors of phosphorus sites in 4-fold coordination emerges as a local (pseudo)plane rather than the directions of the P-element bond directions, irrespective of the chemical nature of the specimen.

**Acknowledgment.** Financial support of our work by the Deutsche Forschungsgemeinschaft is gratefully acknowledged. We thank Bruker Biospin GmbH, Rheinstetten, for providing generous access to the DSX 500 NMR spectrometer, F. W. Heinemann, Erlangen, for making the single-crystal X-ray diffraction data of **2** available to us, and O. J. Price, Exeter, for helping with some simulations.

## References and Notes

(1) Dusold, S.; Klaus, E.; Sebald, A.; Bak, M.; Nielsen, N. C. *J. Am. Chem. Soc*. **1997**, *119*, 7121.
(2) Davies, J. A.; Dutremez, S. *Coord. Chem Rev*. **1992**, *114*, 61.
(3) Fazlur-Rahman, A. K.; Verkade, J. G. *Inorg. Chem*. **1992**, *31*, 5331.
(4) Geipel, F.; Heinemann, F. W.; Sellmann, D. Unpublished work.
(5) Sebald, A. MAS and CP/MAS NMR of Less Common Spin-1/2 Nuclei. In *NMR Basic Principles and Progress*; Springer-Verlag: Berlin, 1994; Vol. 31, pp 91−131.
(6) Challoner, R.; Sebald, A. *Solid State Nucl. Magn. Reson.* **1995**, *4*, 39.
(7) Nielsen, N. C. N.; Creuzet, F.; Griffin, R. G.; Levitt, M. H. *J. Chem. Phys.* **1992**, *96*, 5668.
(8) Ernst, R. R.; Bodenhausen, G.; Wokaun, A. *Principles of Nuclear Magnetic Resonance in One and Two Dimensions*; Clarendon Press: Oxford, U.K., 1987.
(9) Levitt, M. H. *J. Magn. Reson.* **1997**, *126*, 164.
(10) Haeberlen, U. *Advances in Magnetic Resonance*, Supplement 1; Academic Press: New York, 1976.
(11) Edmonds, A. R. *Angular momentum in quantum mechanics*; Princeton University Press: Princeton, NJ, 1974.
(12) Bechmann, M.; Sebald, A. *J. Magn. Reson.* **2005**, *173*, 296.
(13) Dusold, S.; Milius, W.; Sebald, A. *J. Magn. Reson.* **1998**, *135*, 500.
(14) Dusold, S.; Maisel, H.; Sebald, A. *J. Magn. Reson*. **1999**, *141*, 78.
(15) Bechmann, M.; Dusold, S.; Förster, H.; Haeberlen, U.; Lis, T.; Sebald, A.; Stumber, M. *Mol. Phys*. **2000**, *98*, 605.
(16) Dusold, S.; Sebald, A. *Mol. Phys*. **1998**, *95*, 1237.
(17) Dusold, S.; Sebald, A. Dipolar Recoupling under Magic-Angle Spinning Conditions. In *Annual Reports on NMR Spectroscopy*; Academic Press: London, 2000; Vol. 41, pp 185−264.
(18) Bak, M.; Nielsen, N. C. *J. Magn. Reson*. **1997**, *125*, 132.
(19) Maricq, M. M.; Waugh, J. S. *J. Chem. Phys*. **1979**, *70*, 3300.
(20) Nakai, T.; McDowell, C. A. *Mol. Phys*. **1992**, *77*, 569.
(21) Nakai, T.; McDowell, C. A. *J. Chem. Phys*. **1992**, *96*, 3452.
(22) Miura, H.; Terao, T.; Saika, A. *J. Chem. Phys*. **1986**, *85*, 2458.
(23) Marichal, C.; Sebald, A. *Chem. Phys. Lett*. **1998**, *286*, 298.
(24) Hoffmann, A.; Schnell, I. *ChemPhysChem*. **2004**, *5*, 966.
(25) Crystal-structure determinations of several closely related Pt(II) complexes with a *cis*-$S_2PtP_2$ core have been reported in the literature: Fenn, R. H.; Segrott, G. R. *J. Chem. Soc. A* **1970**, 2781. Lin, I. J. B.; Chen, H. W.; Fackler, J. P. *Inorg. Chem*. **1978**, *17*, 394. Dudis, D.; Fackler, J. P. *Inorg. Chem*. **1982**, *21*, 3577. Bryan, S. A.; Roundhill, D. M. *Acta Crystallogr. C* **1983**, *39*, 184. Briant, C. E.; Calhorda, M. J.; Hor, T. S. A.; Howells, N. D.; Mingos, D. M. P. *J. Chem. Soc., Dalton Trans*. **1983**, 1325. Shaver, A.; Lai, R. D.; Bird, P. H.; Wickramasinghe, W. *Can. J. Chem*. **1985**, *63*, 2555. Vicente, R.; Ribas, J.; Solans, X.; Font-Altaba, M.; Mari, A.; de Loth, P.; Cassoux, P. *Inorg. Chim. Acta* **1987**, *132*, 229. Weigand, W.; Bosl, G.; Polborn, K. *Chem. Ber*. **1990**, *123*, 1339. Dudis, D. S.; King, C.; Fackler, J. P. *Inorg. Chim. Acta* **1991**, *181*, 99. Bevilacqua, J. M.; Zuleta, J. A.; Eisenberg, R. *Inorg. Chem*. **1994**, *33*, 258. Belluco, U.; Bertani, R.; Michelin, R. A.; Mozzon, M.; Bombieri, G.; Benetollo, F. *Gazz. Chim. Ital*. **1994**, *124*, 487. Chen, Q.; Boeheim, F.; Dabrowiak, J.; Zubieta, J. *Inorg. Chim. Acta* **1994**, *216*, 83.
(26) Ashbrook, S. E.; Wimperis, S. *High-resolution NMR of quadrupolar nuclei in solids: The satellite-transition magic angle spinning (STMAS) experiment*. *Prog. Nucl. Magn. Reson. Spectrosc.* **2004**, *45*, 53−108.
(27) Kohler, S. J.; Ellett, D. J., jr.; Klein, M. P. *J. Chem. Phys*. **1976**, *64*, 4451.
(28) Kohler, S. J.; Klein, M. P. *Biochem*. **1976**, *15*, 967.
(29) Kohler, S. J.; Klein, M. P. *J. Am. Chem. Soc*. **1977**, *99*, 8290.
(30) Herzfeld, G.; Griffin, R. G.; Haberkorn, R. A. *Biochem*. **1978**, *17*, 2711.
(31) Tutunjian, P. N.; Waugh, J. S. *J. Chem. Phys*. **1982**, *76*, 1223.
(32) Tutunjian, P. N.; Tropp, J.; Waugh, J. S. *J. Am. Chem. Soc*. **1983**, *105*, 4848.
(33) Naito, A.; Sastry, D. L.; McDowell, C. A. *Chem. Phys. Lett*. **1985**, *115*, 19.
(34) Hauser, H.; Radloff, C.; Ernst, R. R.; Sundell, S.; Pascher, I. *J. Am. Chem. Soc*. **1988**, *110*, 1054.
(35) McDowell, C. A.; Naito, A.; Sastry, D. L.; Takegoshi, K. *J. Magn. Reson*. **1988**, *78*, 498.
(36) Ermark, F.; Topic, B.; Haeberlen, U.; Blinc, R. *J. Phys.: Condens. Matter* **1989**, *1*, *5489*.
(37) Eichele, K.; Wasylishen, R. E. *J. Phys. Chem*. **1994**, *98*, 3108.
(38) Eichele K.; Wu, G.; Wasylishen, R. E.; Britten, J. F. *J. Phys. Chem*. **1995**, *99*, 1030.
(39) Lumsden, M. D.; Wasylishen, R. E.; Britten, J. F. *J. Phys. Chem*. **1995**, *99*, 16602.
(40) Eichele K.; Wasylishen, R. E.; Maitra, K.; Nelson, J. H.; Britten, J. F. *Inorg. Chem*. **1997**, *36*, 3539.
(41) Jensen, T. R.; Hazell, R. G.; Vosegaard, T.; Jakobsen, H. J. *Inorg. Chem*. **2000**, *39*, 2026.
(42) Gee, M.; Wasylishen, R. E.; Eichele, K.; *J. Phys. Chem*. *A* **2000**, *104*, 4598.
(43) Grossmann, G.; Scheller, D.; Malkina, O. L.; Malkin, V. G.; Zahn, G.; Schmidt, H.; Haeberlen, U. *Solid State Nucl. Magn. Reson*. **2000**, *17*, 22.
(44) Eichele, K.; Wasylishen, R. E.; Corrigan, J. F.; Taylor, N. J.; Carty, A. J.; Feindel, K. W.; Benard, G. M. *J. Am. Chem. Soc*. **2002**, *124*, 1541.
(45) Power, W. P.; Wasylishen, R. E. *Inorg. Chem*. **1992**, *31*, 2176.
(46) Eichele, K.; Ossenkamp, G. C.; Wasylishen, R. E.; Cameron, T. S. *Inorg. Chem*. **1999**, *38*, 639.
(47) Bernard, G. M.; Wu, G.; Lumsden, M. D.; Wasylishen, R. E.; Maigrot, N.; Charrier, C.; Mathey, F. *J. Phys. Chem*. *A* **1999**, *103*, 1029.
(48) Potrzebowski, M. J.; Assfeld, X.; Ganicz, K.; Olejniczak, S.; Cartier, A.; Garsiennet, C.; Tekely, P. *J. Am. Chem. Soc*. **2003**, *125*, 4223.